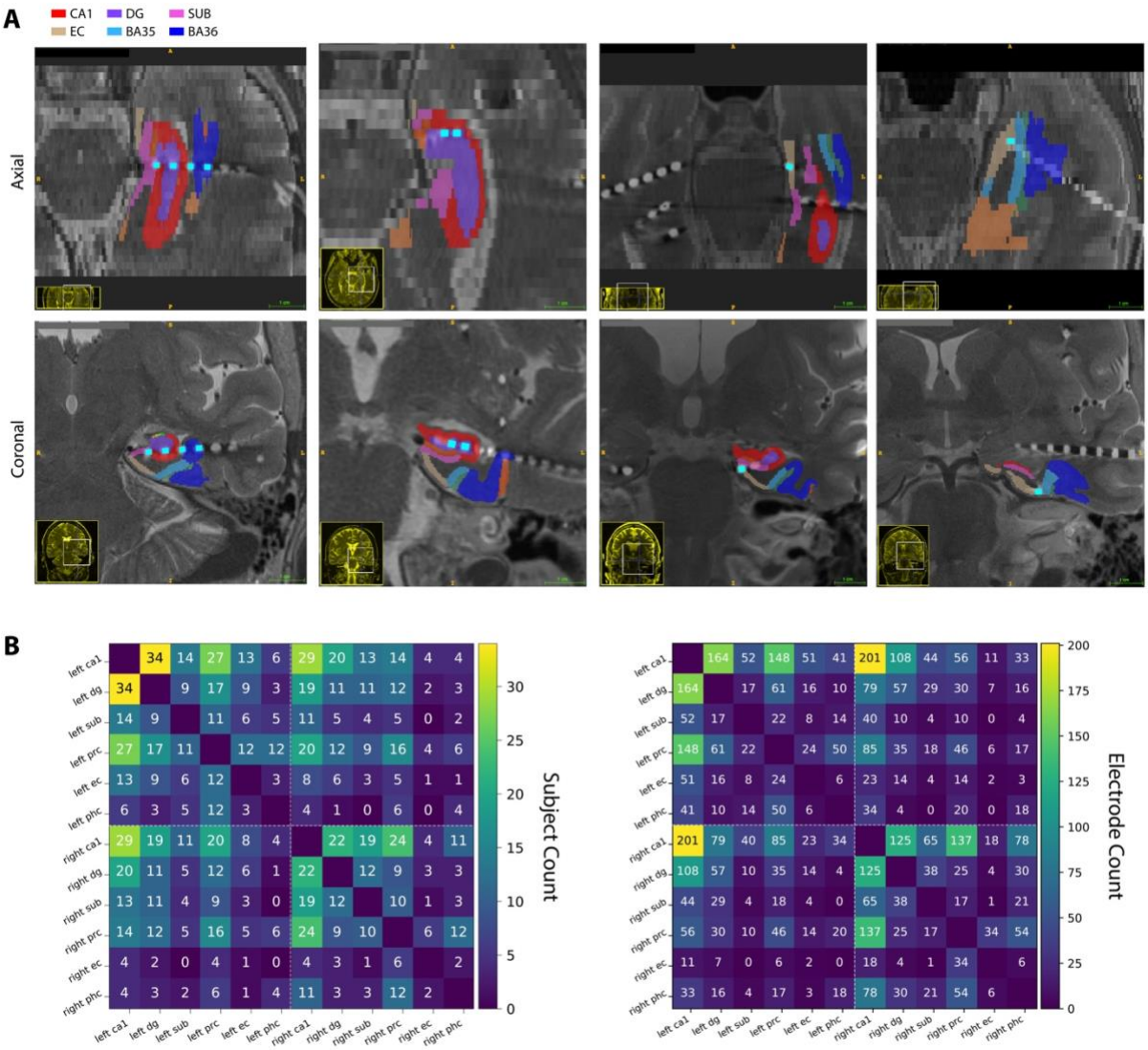

Figure S1. Localization of depth electrodes to MTL subregions. Related to Figure 1. **A.** Example placement of depth electrodes in MTL subregions. Post-operative CT scans are coregistered to preoperative T2 MRI and overlaid with segmentations as derived from ASHS. Blue squares indicate the approximate to-scale size of recording contacts; see Supplemental Table 1 for contact geometries. Top row depicts an axial view, bottom row depicts a coronal view of the same electrode. Subregion labels are as follows: DG, dentate gyrus; EC, entorhinal cortex, SUB, subiculum; BA35/BA36, perirhinal cortex. **B.** Adjacency matrix representation of the number of subjects (left) or number of recording contacts (right) contributing to each region-pair. Warm colors indicate greater numbers of subjects. Exact counts are displayed in each cell of the matrix, which is symmetric across the diagonal. Any pair with fewer than 5 subjects was excluded from all analyses.

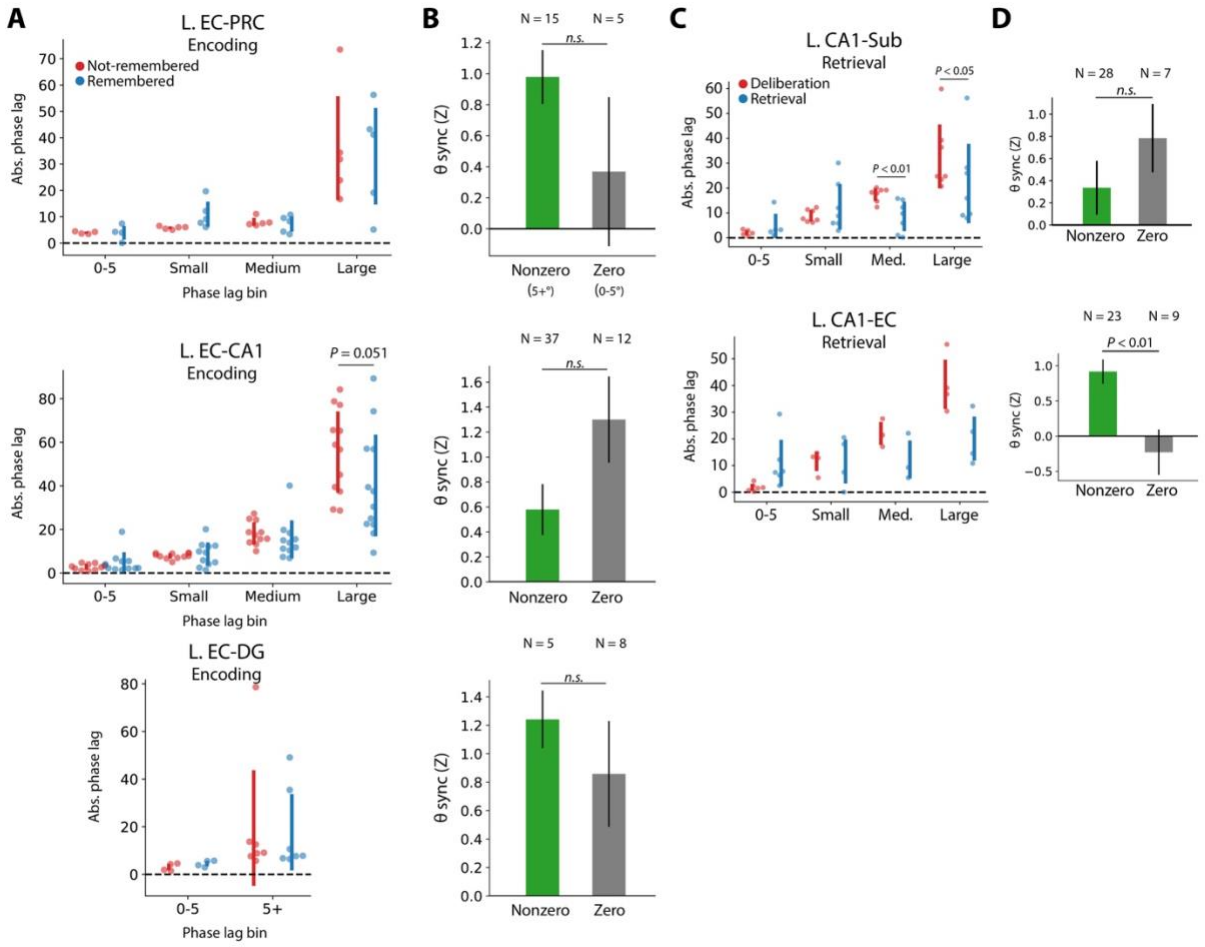

Figure S2. Theta phase lag differentials between memory states. Related to Figure 4 and Figure 5.

A. For each key inter-regional connection depicted in Figure 4, absolute mean theta phase lags are plotted for each electrode pair that exhibits a significantly nonuniform phase lag distribution (Rayleigh test, $P < 0.05$). Absolute lags were measured by finding the shortest rotational distance to either 0 degrees or 180 degrees. Phase lags were measured at the maximal time window and theta frequency as depicted in Figure 4. Mean phase lags were divided into four bins, 0-5 degrees (representing approximately zero lag), and terciles of the remaining lags. (Left EC vs. left DG, bottom row, was divided into two bins due to a small number of contributing electrode pairs). For each bin, mean phase lags are plotted for the not-remembered (red) and remembered (blue) trials separately. Vertical bars indicate +/- 1 standard deviation of the data. In general, phase lags are smaller in successful encoding trials, though not significantly so unless indicated (paired *t*-test). **B.** Relative theta synchronization (z-score) was compared between electrode pairs with zero lag (0-5 degrees) and nonzero lag (5+ degrees) in the successful encoding condition (a 10 degree cutoff was used in the EC/DG connection due to smaller sample size). No significant differences were observed between synchronization in zero and nonzero lagged pairs (2-sample *t*-test, $P > 0.05$). **C.** Same as (A), for key connections during the retrieval period. Significant retrieval-associated decreases in phase lag were noted for medium and large lags in the left CA1 vs. left subiculum connection. **D.** Same as (B), for key connections during the retrieval period.

Nonzero lagged pairs exhibited significantly greater synchronization between left CA1 and left EC ($P < 0.01$).

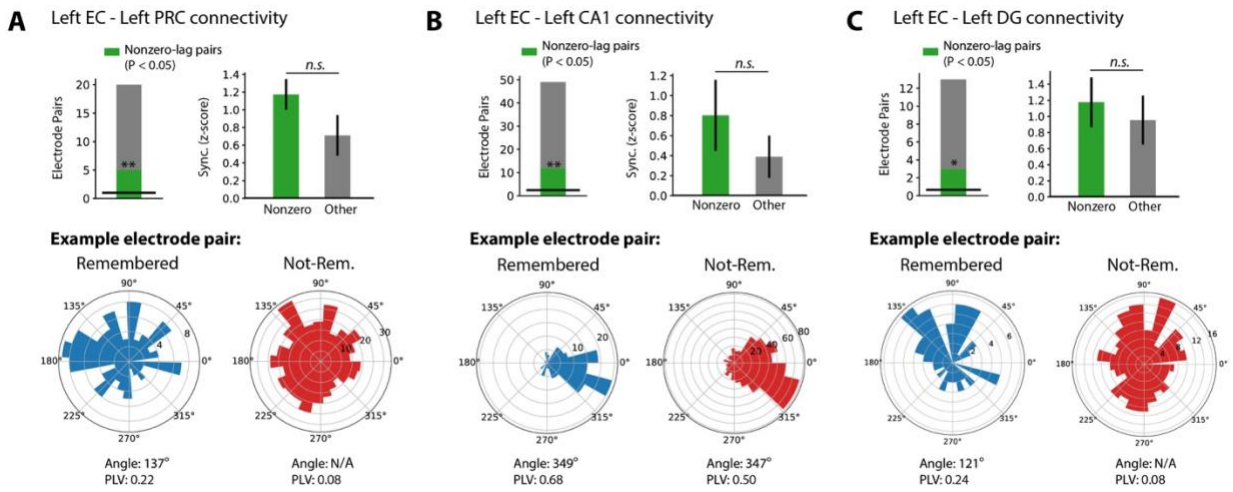

Figure S3. Circular *m*-test for zero-lagged pairs. Related to Figure 4.
A-C. To confirm further whether synchronization differs between electrode pairs with zero and nonzero lags, we used the circular one-sample *m*-test (pycircstat; Berens, et al. 2014) to ask whether a given electrode pair exhibits a distribution phase lags that differ significantly from zero or 180 degrees ($P < 0.05$). Note that rejecting the null hypothesis means a distribution differs from zero; failure to reject the null does not mean a distribution is centered at zero. *Top left:* A significantly greater number of pairs exhibit nonzero lags (green bar) than would be expected by chance, under the null hypothesis that all pairs are corrupted by zero-lag volume conduction (binomial test, $^{**}P < 0.01$; $^{*}P < 0.05$). *Top right:* No significant differences were observed between memory-related synchronization among pairs with nonzero lags and all others (2-sample *t*-test, $P > 0.05$). *Bottom*: Phase lag distributions from an example electrode pair. Blue indicates lags during successful encoding trials, red are lags from unsuccessful encoding trials. As in Figure S2, phase lags are assessed at the time and theta frequency of maximal synchronization (see Figure 3). Error bars show +/- 1 SEM.

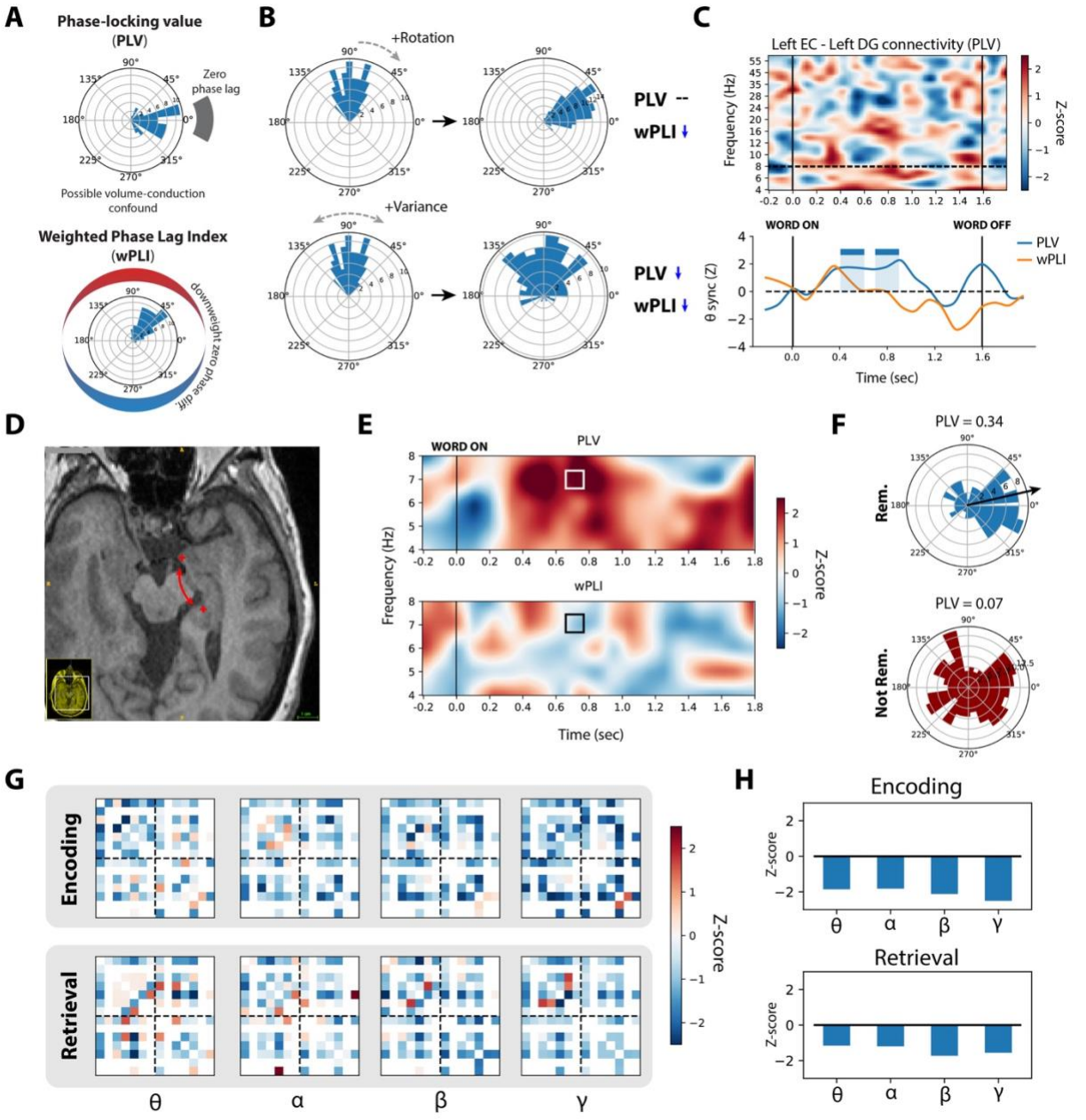

Figure S4. Weighted phase-lag index (wPLI) analysis. Related to Figure 4 and Figure 7.
A. PLV reflects the consistency of phase differences across trials, indicated in example data as clustered phase lags around zero (left). The wPLI works similarly, but downweights the contribution of phase lags near the zero axis, which may reflect volume conduction (right). Accordingly, stronger connectivity is observed if phase lags are clustered around a direction far from zero (or 180 degrees). **B.** As demonstrated using simulated data, the wPLI can differ between conditions for two reasons. First, depicted in the top row, well-clustered phase lags can rotate toward zero – decreasing wPLI which downweights phase lags closer to zero to account for volume conduction. In this case, the PLV will remain unchanged. Second, depicted in the bottom row, the variance of a nonzero phase lag distribution can increase between conditions, causing decreases in PLV and wPLI. **C.** *Top*: Time-frequency plot of PLV synchronization between left EC and left DG in the encoding contrast, averaged across subjects. Red colors indicate relative synchronization in remembered versus not-remembered trials, blue colors indicate relative

desynchronization. Vertical black lines indicate word onset and offset, dotted horizontal line indicates the max theta frequency considered for connectivity analyses. *Bottom*: In non-overlapping 100 ms windows, PLV (blue) and wPLI (orange) values are averaged across all theta frequencies, yielding a synchronization timeseries. Any two consecutive 100 ms windows with synchronization significantly greater than chance ($P < 0.05$) are marked as significant with blue or orange colored rectangles (see Methods for details). In this region-pair, PLV is significant from 400-600 ms and 700-900 ms after word onset. **D.** Axial T1-weighted MRI slice depicting electrode locations for a representative pair spanning the left DG and EC. **E.** Time-frequency plots for the indicated electrode pair, theta frequencies only. Top row shows PLV synchronization during successful encoding, bottom row shows wPLI synchronization. The considered interval and frequency for phase lags in (E) is marked with a square. **F.** For the highlighted frequency and interval, phase lags were binned according to whether the trial was later remembered (blue) or not-remembered (red). The mean direction of the clustered remembered trials is 9.7 degrees (PLV = 0.34), indicated with the black arrow. Not-remembered trials are unclustered, as reflected by a low PLV of 0.07. **G.** Average wPLI was computed for each pair of MTL subregions across the encoding and retrieval intervals. Adjacency matrices depict the difference in wPLI between remembered and not-remembered conditions. **H.** Overall network-wide synchronization was computed by averaging the connection weights in (G). Memory-related decreases in wPLI are observed at all frequency bands.

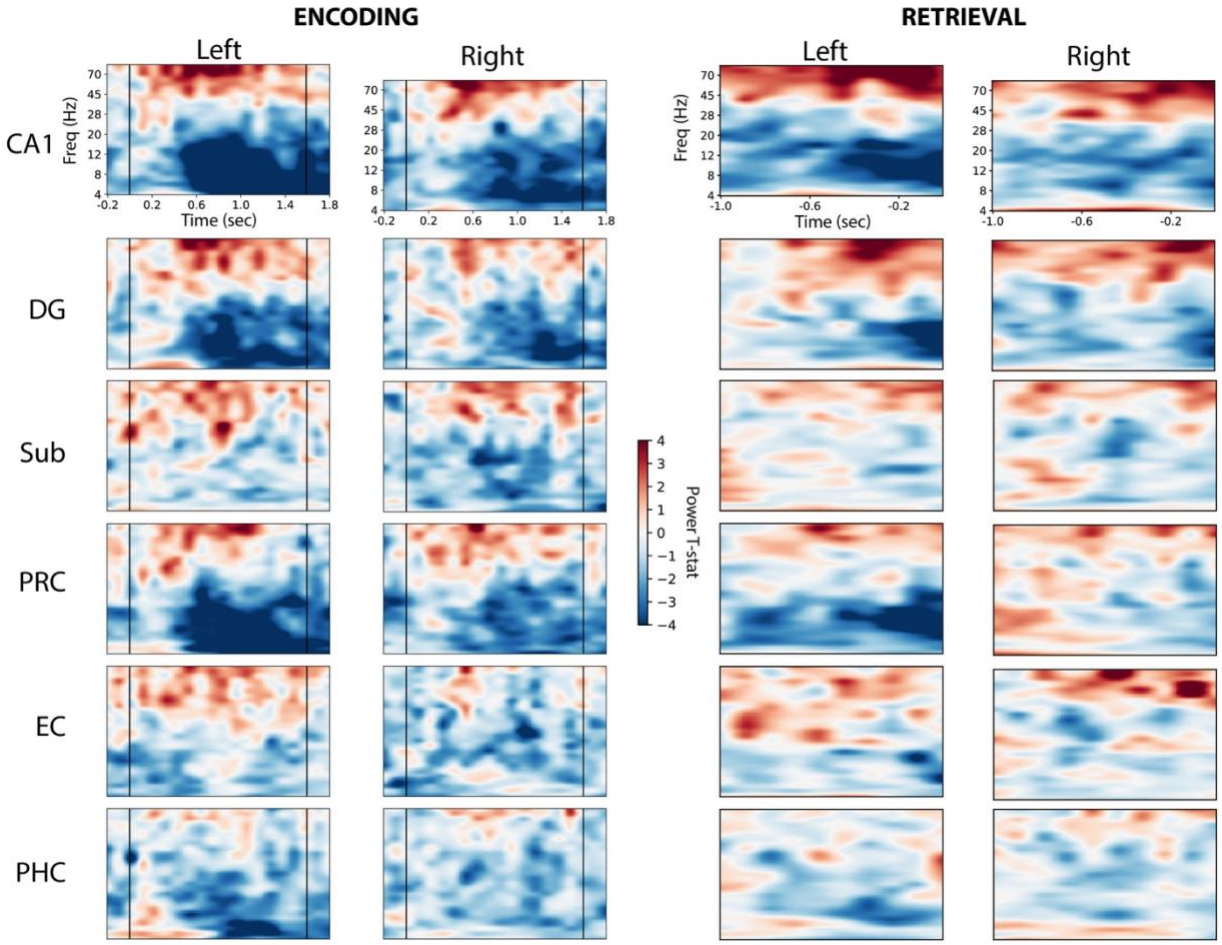

Figure S5. Memory-related spectral power at all MTL subregions. Related to Figure 6. For each MTL subregion, the spectral power during successful vs. unsuccessful encoding or retrieval epochs was measured for frequencies spanning 4-90 Hz. *Left*: Time-frequency plots of the successful vs. unsuccessful encoding contrast. Vertical bars indicate word onset and offset. *Right:* Contrast of successful retrieval vs. deliberation epochs. Retrieval occurs at 0.0 seconds, or the rightmost edge of each plot. Subregion acronyms are defined in Figure S1.

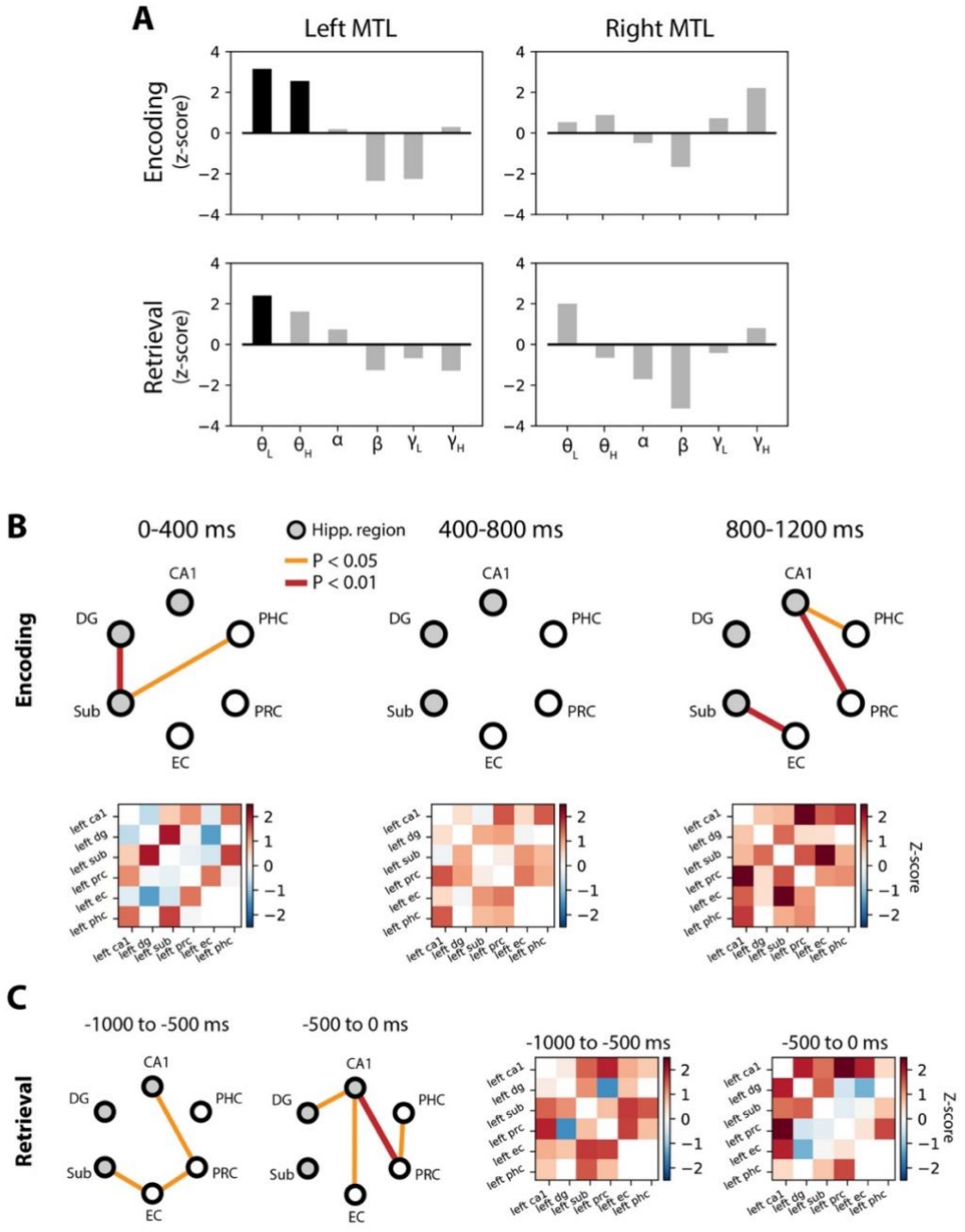

Figure S6. Analysis of synchronization in extended frequency bands. Related to Figure 7. **A.** Low-theta (1-3 Hz) and high-gamma (70-90 Hz) bands were analyzed for network-wide synchronization in the right and left MTL, for the encoding and retrieval contrasts (see Figure 7 for more detail). Significant (corrected permuted $P < 0.05$) network-wide synchronization was found in the low-theta band in the left MTL during encoding and retrieval. No other frequency bands demonstrated significant memory-related synchronization. **B.** Significant low-theta intra-MTL connections during early, middle, and late encoding, as depicted in Figure 3A. **C.** Same as (B) and Figure 3B, but for early and late retrieval periods.

Table S1. Depth electrode dimensions and spacing. Related to Figure 1 and STAR Methods.

Device Name	Manufacturer	Exposed Contact Diameter (mm)	Exposed Contact Length (mm)	Contact Spacing
Macro-Micro Depth Electrodes	AdTech	1.28 (macro)	1.57 (macro)	5-10mm
Spencer Probe Depth Electrode	Adtech	1.12	2.4	5mm
Spencer Probe Depth Electrode	AdTech	1.96	1.27	5-10mm
Behnke-Fried Electrode	AdTech	1.28	1.57	5mm
Spencer Probe Depth Electrode	AdTech	0.86	2.29	4-8mm
Depthalon	PMT	0.8	2	3.5mm
Spencer Probe Depth Electrode	AdTech	1.12	1.32	2.2mm
PMT Macro-Micro NINDS	PMT	0.8	1.4	7mm